Climate change decouples oceanic primary and export productivity and organic carbon burial

Cristina Lopes[a,b,1], Michal Kucera[c], and Alan C. Mix[d]

[a]IPMA, Instituto Português do Mar e da Atmosfera, 1749-077 Lisbon, Portugal; [b]CIMAR, Centro de Investigação Marinha e Ambiental, Rua dos Bragas, 4050-123 Porto, Portugal; [c]MARUM, Center for Marine Environmental Sciences, University of Bremen, DE-28359 Bremen, Germany; and [d]CEOAS, College of Earth, Ocean, and Atmospheric Sciences, Oregon State University, Corvallis, OR 97331

Edited by James P. Kennett, University of California, Santa Barbara, CA, and approved October 27, 2014 (received for review June 5, 2014)

Understanding responses of oceanic primary productivity, carbon export, and burial to climate change is essential for model-based projection of biological feedbacks in a high-CO_2 world. Here we compare estimates of productivity based on the composition of fossil diatom floras with organic carbon burial off Oregon in the Northeast Pacific across a large climatic transition at the last glacial termination. Although estimated primary productivity was highest during the Last Glacial Maximum, carbon burial was lowest, reflecting reduced preservation linked to low sedimentation rates. A diatom size index further points to a glacial decrease (and deglacial increase) in the fraction of fixed carbon that was exported, inferred to reflect expansion, and contraction, of subpolar ecosystems that today favor smaller plankton. Thus, in contrast to models that link remineralization of carbon to temperature, in the Northeast Pacific, we find dominant ecosystem and sea floor control such that intervals of warming climate had more efficient carbon export and higher carbon burial despite falling primary productivity.

organic carbon | export productivity | glacial-interglacial | diatoms | biological pump

Photosynthetic activity of marine algae fixes dissolved inorganic carbon into biomass. A fraction of this biomass is exported and remineralized or buried in the deep ocean (1). The efficiency of this process, known as the biological pump, may vary among oceanic regions (2) and on geological time scales (3). Biogeochemical models can be used to predict the future behavior of the carbon cycle; however, their efficacy depends on how they calculate primary and export production and remineralization (4). Some models remineralize carbon in the water column based on temperature and sinking velocity (5), and others are tuned to the modern depth distribution of sediment trap fluxes (6). It remains to be established whether these parameterizations are stable across climate transitions and whether they include all key determinants of the efficiency of the biological pump.

The geological record provides an opportunity to assess the sensitivity of the biological pump to changing boundary conditions. On geological time scales, organic carbon burial in deep sea sediments is often interpreted as a tracer of productivity (7), and the implied net carbon flux from the surface to the deep ocean has been implicated as one of the key processes explaining lowered atmospheric carbon dioxide levels during glacial times (8). However, reconstructions of productivity based on organic carbon burial have been questioned based on sensitivity to diagenesis within the sediment, either related to oxygen availability (9) or sorption on mineral surfaces (10, 11). Conflicts among estimates of biological production based on different proxies have also been noted (12–14). Resolution of these disagreements, and better understanding of the interactions between climate and the carbon cycle, requires new proxy approaches that compare the state of the photosynthesizing plankton community, export of carbon to the deep sea, and rates of carbon burial on the basis of independent indicators.

Materials and Methods

We estimate mean annual primary productivity (PPa) quantitatively based on the composition of diatom floras in marine sediments of the Northeast Pacific, the phytoplankton group most closely associated with carbon fixation here. We assess changes in carbon export efficiency (based on a diatom size index; Tables S1 and S2 and Dataset S1) and burial efficiency (based on organic carbon mass accumulation rates) over the last ∼30 ka at one of the two locations representing coastal and open-ocean high productivity upwelling regimes (Fig. 1). Under the coastal upwelling regime, the record from Ocean Drilling Program (ODP) site 1019 (41.683°N, 124.933°W, 978 m depth) is combined with adjacent core MD02-2499 (41.683°N, 124.940°W, 904 m depth; Fig. S1). The region of seasonal open-ocean upwelling system (Fig. S2) driven by wind-stress curl (15) is represented by core W8709-13PC (42.117°N, 125.75°W, 2712 m depth) from the eastern flank of the Gorda Ridge, ∼220 km offshore.

For cores ODP 1019 and MD02-2499, a radiocarbon-based age model (16, 17) is further tuned by correlation of benthic $\delta^{18}O$ to the radiocarbon-dated W8709-13PC (15, 17). The chronology of core W8709-13PC is based on 40 planktonic foraminifera radiocarbon dates including data from ref. 18 and three additional post-LGM dates (Table S3). Sedimentation rates for this core and uncertainties were estimated by Monte Carlo simulation in fixed increments (Table S3). This approach resolves the main paleoclimatic transitions but avoids amplification of uncertainties between closely spaced pairs of individual dates. Organic carbon burial rates combine sedimentation rates, dry bulk density, and measurements of organic carbon concentration. The coastal upwelling site includes a large contribution of organic matter from terrestrial sources (19), and this precludes meaningful calculation of marine organic carbon burial and export efficiency as a fraction of primary production; nevertheless, this coastal site is used to estimate PPa from diatom floras and verifies that productivity patterns seen in the offshore site also apply to the coastal upwelling system.

We previously developed a statistical transfer function to estimate PPa from diatom species relative abundance, including freshwater diatoms, based on unimodal maximum likelihood (ML) methods (20). During the Last Glacial

Significance

Climate and ecosystem changes in the Northeast Pacific decoupled primary and export productivity and organic carbon burial during climate warming of the last deglaciation. These findings challenge and clarify the meaning of paleoceanographic proxies of productivity and provide key constraints for modeling of the ocean's biological pump as a potential carbon feedback mechanism associated with large-scale climate change. To our knowledge, this is the first clear demonstration that primary productivity, export productivity, and carbon burial are significantly decoupled under scenarios of large-scale climate change. This is an important constraint on biogeochemical carbon cycle models, which generally assume such changes covary.

Author contributions: C.L., M.K., and A.C.M. analyzed data; C.L., M.K., and A.C.M. wrote the paper.

The authors declare no conflict of interest.

This article is a PNAS Direct Submission.

See Commentary on page 306.

[1]To whom correspondence should be addressed. Email: cristina.c.lopes@gmail.com.

This article contains supporting information online at www.pnas.org/lookup/suppl/doi:10.1073/pnas.1410480111/-/DCSupplemental.

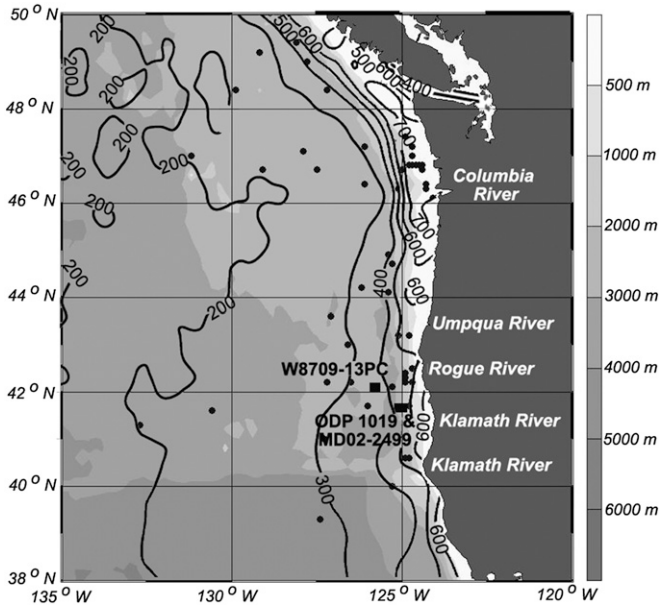

Fig. 1. Study area. Circles indicate the position of core top samples used to derive the productivity transfer function; squares mark the position of downcore records. Gray shading shows bathymetry. Contours show the spatial pattern of modern mean annual primary productivity (gC/m^2/y) from ref. 20.

Maximum, high abundance of freshwater diatoms in marine sediments sourced from the Columbia River (15) creates a no-analog condition in the published scheme. To circumvent this no-analog condition, here we exclude freshwater diatoms from the analysis (i.e., we put closure around marine diatoms) and recalibrate the transfer functions. We further compare PPa estimates based on ML approaches with an independent, nonparametric approach of artificial neural networks (ANN; details in *SI Materials and Methods*; Fig. S3). The ML transfer function for PPa has a cross-validated jackknifed r^2 of 0.75 and a root mean square error of prediction (RMSEP) uncertainty of 155 grams carbon per square meter per year (gC/m^2/y), 15% of the total calibration range of 197–1243 gC/m^2/y. The ANN estimator for PPa has an r^2 (here expressed as between observed and estimated values; ANN does not give a jackknifed r^2) of 0.92 and an RMSE uncertainty of 104 gC/m^2/y (10% of the calibration range).

Results and Discussion

Estimates of core-top PPa based on ML and ANN at site ODP 1019 (475 ± 104 and 345 ± 155 gC/m^2/y, respectively) are consistent with the modern observed values (426 gC/m^2/y) (21). The youngest (mid-Holocene) PPa reconstructions for core W8709-13PC (564 ± 104 and 454 ± 155 gC/m^2/y for ML and ANN, respectively) are slightly higher than the modern atlas value of 351 gC/m^2/y. Both methods estimate PPa during glacial times about double that of the late Holocene; the ML estimates display higher variance than the ANN estimates at both core sites during the glacial interval (Fig. 2 *A* and *B*). PPa decreases abruptly between ∼17 and 16 ka and again between ∼13 and ∼11 ka, which is coincident with times of rapidly increasing atmospheric CO_2 (22).

To assess oceanographic mechanisms driving productivity change, we calculated a diatom-based upwelling index (Fig. 2*C* and *SI Materials and Methods*) in a manner similar to ref. 23, but excluding freshwater diatoms as these track river input (15) (Fig. 2*D*). A diatom size index (Fig. 2*E*) traces the efficiency of carbon export from the sea surface. Larger diatoms today are associated with high-export coastal upwelling systems replete with iron, whereas small diatoms are associated with low-export open ocean systems that are iron limited (24). As expected, this index is generally higher at our coastal upwelling site (ODP 1019 and MD02-2499) than offshore (W8709-13PC). The offshore Oregon system today is under mild iron stress, such that iron availability regulates the magnitude of phytoplankton blooms (25). Although some of the peaks in PPa are coincident with peaks in the upwelling index, in general, the upwelling index is lower during the LGM, consistent with a southward shift of the subpolar gyre (14). Substantially higher freshwater input documented during glacial time, especially during flood events (Fig. 2*D*) (15), may also contribute nutrients including silica and iron that are expected drivers of productivity. Overall, high glacial primary productivity tracks long-term increases in apparent river inputs, but in detail, reconstructed PPa highs do not match the individual peaks in freshwater diatom abundance, so the connection is likely indirect. Although not constrained here, such an indirect connection may reflect the tendency of river-borne iron in colloids to flocculate and sink quickly on encountering salt water (26); suboxic remobilization of iron from accumulation sites in shelf sediments makes it available to the biota during the upwelling season (27). Relatively low flooded shelf area during the glacial maximum may have limited this mechanism for iron fertilization despite strong regional river input. Thus, high primary productivity in the region may reflect nitrate, phosphate, and silicic acid inputs from strong river fluxes, whereas relatively low export may have reflected iron limitation.

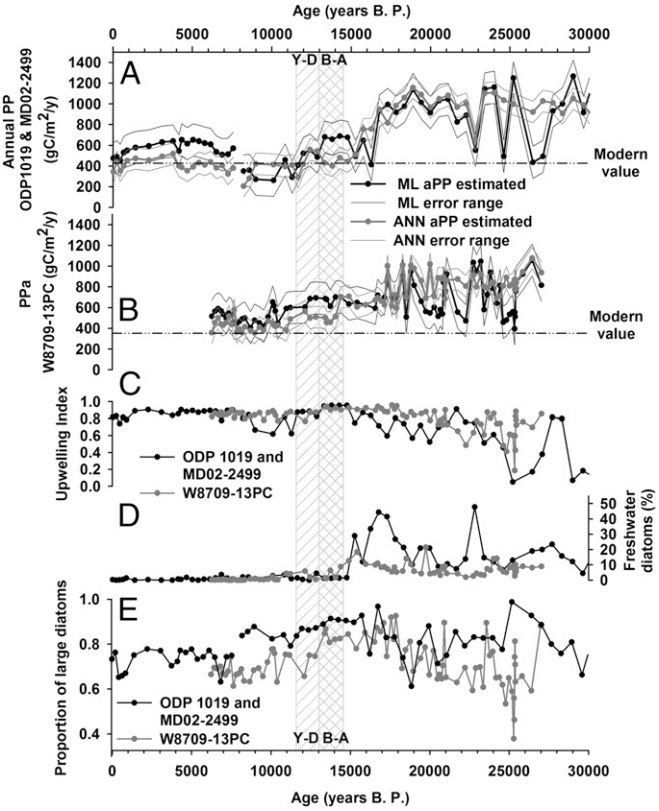

Fig. 2. Diatom-based paleoenvironmental indices across the last glacial termination in the Northeastern Pacific. For derivation, see Dataset S2. PPa reconstructions for (*A*) ODP 1019 and MD02-2499 (ML in black and ANN in gray) and (*B*) W8709-13PC (ML in black and ANN in gray); thin lines indicate the uncertainty envelope of each method. (*C*) Upwelling index based on Q-mode factor analysis for MD02-2499 (black) and W8709-13PC (gray). (*D*) Abundance of freshwater diatoms as a percentage of total diatoms (a proxy for river discharge) at ODP 1019 and MD02-2499 (black) and W8709-13PC (gray). (*E*) Percentage of large diatoms [relative to total marine diatoms; a proxy for export efficiency at ODP 1019 and MD02-2499 (black) and W8709-13PC (gray)]. Age model's details are in *SI Materials and Methods*.

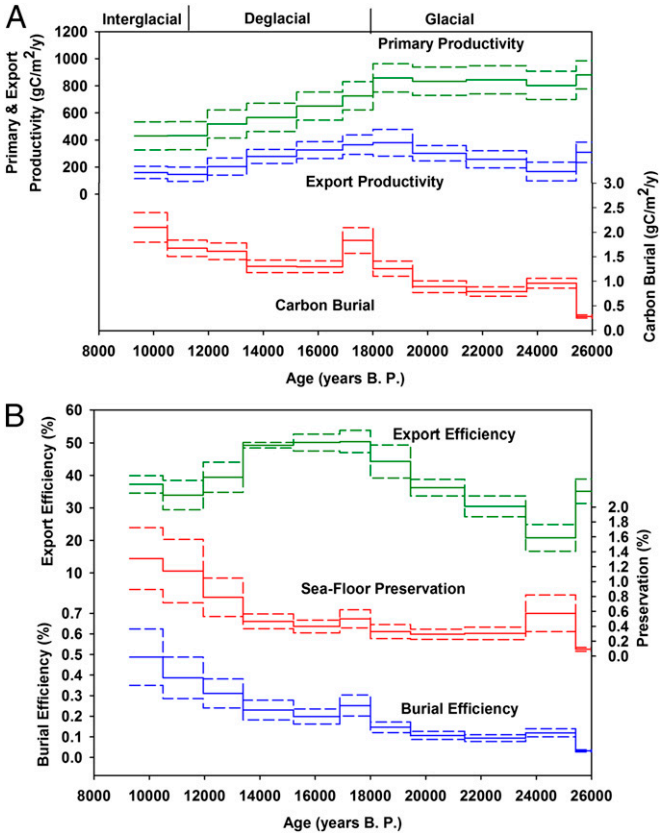

Fig. 3. Variations in components of the biological pump across the glacial termination at site W8709-13PC, calculated in 30-cm averaged intervals. (*A*) Primary productivity (PPa), export productivity (EP), and organic carbon burial (OCB) averaged in 30-cm nonoverlapping consecutive intervals with uncertainty estimates (Dataset S3). (*B*) Export efficiency (EP/PPa), burial efficiency (OCB/PPa), and seafloor preservation of organic carbon (OCB/EP) expressed as percentages. Uncertainties are ±1σ (Dataset S4).

To assess temporal relationships in carbon fluxes and burial rates, we average all productivity and burial parameters within nonoverlapping consecutive 30-cm increments (*SI Materials and Methods*) and scale the diatom size index linearly to export efficiency (i.e., the ratio export/primary productivity) such that it spans a range of 20–50%. This is similar to the modern range of this ratio from the subtropical North Pacific to the high-latitude upwelling systems (28). Although the exact calibration of the export index is uncertain, our results are relatively insensitive to reasonable variations in the scaling. The results indicate that, although the reconstructed PPa in core W8709-13PC was highest during glacial time (Last Glacial Maximum), the inferred export productivity peaked during the deglaciation (including the Bølling-Allerød, Younger Dryas, and Heinrich event 1 intervals) and the observed carbon burial was highest during interglacial (Holocene) time (Fig. 3).

These results indicate that even under an extreme scenario of changes in export productivity, carbon burial across the last termination does not track productivity at our study site; this is also the case for preservation-corrected productivity indices based on an empirical combination of organic carbon contents and sedimentation rate (29), as well as for other common geochemical productivity indices such as opal percentage and accumulation rate and barium concentration and accumulation rate (*SI Materials and Methods* and Figs. S4 and S5). North of our study area, mass accumulation rates of marine organic carbon are controlled primarily by sedimention rates (especially in late glacial time), but also rise during interglacial time when sedimentation rates were lower (30). It is possible that organic carbon-based estimates of export productivity may work in some regions when confounding influences of preservation are relatively small. Thus, it is plausible that organic carbon-based estimates of export productivity may work in some regions where confounding influences are relatively small.

Carbon burial at our Gorda Ridge site is likely dominated by preservation effects, expressed either as sea floor preservation (i.e., OCB/EP) or carbon burial efficiency (i.e., OCB/PPa). Both parameters increased during the deglacial transition when both primary productivity and the inferred export productivity were low (Fig. 3*B*). Across the deglacial transition, carbon burial decreases with increasing primary productivity (Fig. 4*A*) and is unrelated to export productivity (Fig. 4*B*), but shows a strong positive correlation to sedimentation rate (with one outlier, Fig. 4*C*). These findings support hypotheses that link the process of organic carbon preservation either to sorption on mineral surfaces (10, 11) or to integrated oxygen exposure time (9, 31), both of which are influenced directly by sediment accumulation rate. There is no

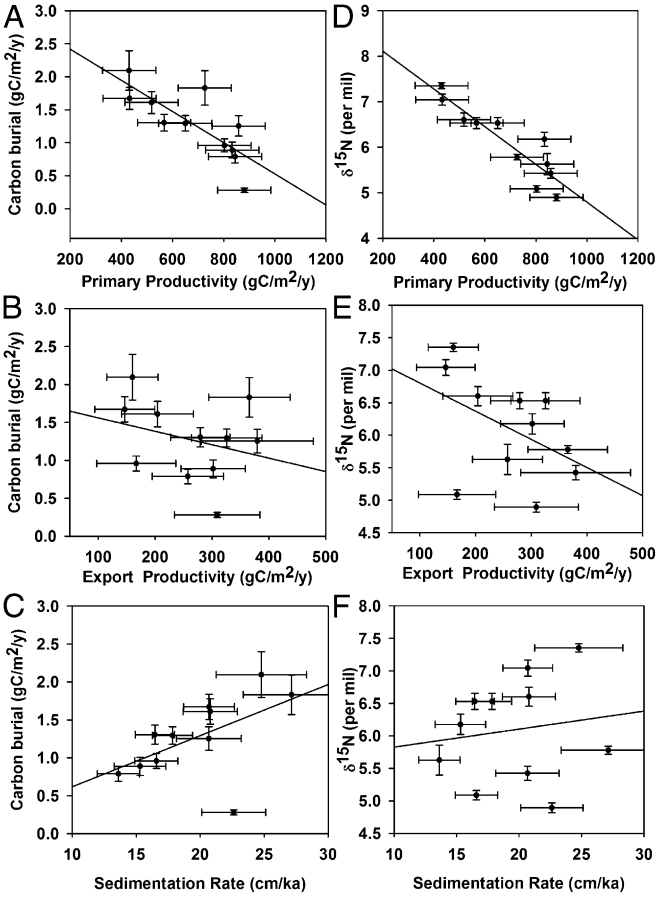

Fig. 4. Determinants of carbon burial across the glacial termination at site W8709-13PC. (*A*) Carbon burial decreases with increasing reconstructed PPa ($r = 0.8$, $P = 0.001$). (*B*) Carbon burial is not significantly correlated to estimated export productivity ($r = 0.3$, $P = 0.18$). (*C*) Carbon burial increases proportional to sedimentation rate ($r = 0.5$, $P = 0.05$), suggesting that preservation effects linked to sedimentation rate, rather than productivity, control carbon burial. (*D*) $\delta^{15}N$ (per mil) decreases with increasing reconstructed PPa ($r = 0.9$, $P < 0.001$). (*E*) $\delta^{15}N$ (per mil) is not significantly correlated to estimated export productivity ($r = 0.2$, $P = 0.28$). (*F*) $\delta^{15}N$ (per mil) does not increase proportionally to sedimentation rate ($r = 0.1$, $P = 0.38$), suggesting that sedimentation rate does not control the $\delta^{15}N$ (per mil) record. All parameters are plotted as means and 1σ uncertainties for nonoverlapping consecutive 30-cm intervals (Dataset S3).

significant correlation between our estimates of PPa from diatom species assemblages and sedimentation rate ($r = -0.3$, $P = 0.18$), implying no obvious artifacts in PPa estimates related to this process.

The apparent changes in export efficiency, which decoupled primary and export production through time, must have plausible ecological controls. In the North Pacific, this likely reflects the transition from a subpolar ecosystem during glacial time (14), similar to that of the modern Alaska Gyre where carbon export is relatively low and primary production is mostly recycled within the water column, to a coastal upwelling system in interglacial time dominated by large diatoms that sink rapidly and are more effective in exporting organic carbon to the deep sea (10, 32). Our PPa estimates are significantly correlated ($r = -0.91$, $P < 0.001$) with δ^{15}N (33). The association of high PPa with low δ^{15}N (Fig. 4*D*) is also consistent with a glacial ecosystem similar to that of the Alaska Gyre, with relatively low fractional nitrate utilization and export efficiency.

Export efficiency peaked during the last deglacial transition, during a time of sea level rise. Such an effect is consistent with hypothesized sources of both particulate and dissolved iron from the continental shelf during sea level rise (16) and from growing hypoxia on the shelf and upper slope during deglacial warming (34, 35). Hypoxia in parts of the North Pacific during the last deglaciation may have been sustained in part by iron feedback that produced an ecological shift to a more efficient exporting ecosystem (36).

Conclusions

Our finding of apparent decoupling between primary productivity, export productivity, and carbon burial has important implications for modeling the responses of the carbon cycle to climate change. For example, one model projects diminished strength of the biological carbon pump under future warming (37); such a feedback process could further increase atmospheric greenhouse gases, but this finding depends on the mechanisms that control export efficiency. Our results discount the importance of temperature as a sole control of carbon remineralization and illustrate dominant ecosystem control of carbon export in the Northeast Pacific. The sense of change in our study is that cold times have lower export efficiency than warm times and that organic carbon burial may be unrelated to change in primary productivity. To the extent that this finding is generally applicable, the biological carbon pump may strengthen in some regions in response to warming. Our data indicate that, at least in the Northeast Pacific and perhaps generally, sediment records of organic carbon burial and other geochemical proxies with preservation sensitive to sedimentation rates cannot be confidently interpreted as a direct proxy for either primary or export production in the past.

ACKNOWLEDGMENTS. This work was funded by Fundação para a Ciência e Tecnologia (FCT) grants to C.L. (PDTC/AAC-CLI/112189/2009; the Panocean project, and SFRH/BPD/26732/2006), FCT, Deutsche Akademische Austauschdienst (DAAD), and Bundesministerium für Bildung und Forschung (BMBF) support through the Program "Acções Integradas Luso-Alemãs/DAAD" to C.L. and M.K., and National Science Foundation Grant 0602395 (Project PaleoVar, to A.C.M.).

1. Falkowski PG, Barber RT, Smetacek V (1998) Biogeochemical controls and feedbacks on ocean primary production. *Science* 281(5374):200–207.
2. Lutz M, Dunbar R, Caldeira K (2002) Regional variability in the vertical flux of particulate organic carbon in the ocean interior. *Global Biogeochem Cycles* 16(3):1037.
3. Raven JA, Falkowski PG (1999) Ocean sinks for atmospheric CO_2. *Plant Cell Environ* 22(6):741–755.
4. Passow U, Carlson CA (2012) The biological pump in a high CO_2 world. *Mar Ecol Prog Ser* 470:249–271.
5. Schmittner A, Oschlies A, Matthews HD, Galbraith ED (2008) Future changes in climate, ocean circulation, ecosystems, and biogeochemical cycling simulated for a business-as-usual, CO_2 emission scenario until year 4000 AD. *Global Biogeochem Cycles* 22(1): GB1013.
6. Bopp L, Le Quere C, Heimann M, Manning AC, Monfray P (2002) Climate-induced oceanic oxygen fluxes: Implications for the contemporary carbon budget. *Global Biogeochem Cycles* 16(2):1022.
7. Kohfeld KE, Le Quéré C, Harrison SP, Anderson RF (2005) Role of marine biology in glacial-interglacial CO_2 cycles. *Science* 308(5718):74–78.
8. Sigman DM, Boyle EA (2000) Glacial/interglacial variations in atmospheric carbon dioxide. *Nature* 407(6806):859–869.
9. Emerson S, Hedges JI (1998) Processes controlling the organic carbon content of open ocean sediments. *Paleoceanography* 3(5):621–634.
10. Keil RG, Montluçon DB, Prahl FG, Hedge JI (1994) Sorptive preservation of labile organic matter in marine sediments. *Nature* 370:549–552.
11. Mayer LM (1994) Surface control of organic carbon accumulation in continental shelf sediments. *Geochim Cosmochim Acta* 58(4):1271–1284.
12. Mix AC (1989) Pleistocene paleoproductivity: Evidence from organic carbon and foraminiferal species. *Productivity of the Ocean: Past and Present*, eds Berger WH, et al. (Wiley, New York), pp 313–340.
13. Sancetta C, Lyle M, Heusser L, Zahn R, Bradbury JP (1992) Late-glacial to Holocene changes in winds, upwelling and seasonal production of the northern California Current System. *Quat Res* 38(3):359–370.
14. Ortiz J, Mix AC, Hostetler S, Kashgarian M (1997) The California Current of the last glacial maximum: Reconstruction at 42°N based on multiple proxies. *Paleoceanography* 12(2):191–205.
15. Lopes C, Mix AC (2009) Pleistocene megafloods in the northeast Pacific. *Geology* 37(1):79–82.
16. Barron JA, Heusser L, Herbert T, Lyle M (2003) High resolution climatic evolution of coastal northern California during the past 16,000 years. *Paleoceanography* 18(1).
17. Mix AC, et al. (1999) Rapid climate oscillations in the northeast Pacific during the last deglaciation reflect Northern and Southern Hemisphere sources. *Mechanisms of Global Climate Change at Millennial Time Scales*, eds Clark PU, Webb RS, Keigwin LD (American Geophysical Union, Washington, DC), AGU Monograph No. 112, pp 127–148.
18. Lund DC, Mix AC, Southon J (2011) Increased ventilation age of the deep northeast Pacific Ocean during the last deglaciation. *Nat Geosci* 4(11):771–774.
19. Lyle M, et al. (1992) Paleoproductivity and carbon burial across the California Current: The multitracers transect, 42°N. *Paleoceanography* 7(3):251–272.
20. Lopes C, Mix AC, Abrantes F (2010) Environmental controls of diatom species in the northeast Pacific. *Palaeogeogr Palaeoclimatol Palaeoecol* 297(1):188–200.
21. Easier Access to Scientific Data (ERDAP), Ocean Watch North Pacific Demonstration Project. Available at coastwatch.pfeg.noaa.gov/erddap/index.html. Accessed April 4, 2012.
22. Parrenin F, et al. (2013) Synchronous change of atmospheric CO_2 and Antarctic temperature during the last deglacial warming. *Science* 339(6123):1060–1063.
23. Lopes C, Mix AC, Abrantes F (2006) Diatoms in northeast Pacific surface sediments as paleoceanographic proxies. *Mar Micropaleontol* 60(1):45–65.
24. Hoffmann LJ, Peeken I, Lochte K, Assmy P, Veldhuis M (2006) Different reaction of Southern Ocean phytoplankton sized classes to iron fertilization. *Limnol Oceanogr* 51(3):1217–1229.
25. Chase Z, van Geen A, Kosro PM, Marra J, Wheeler PA (2002) Iron, nutrient, and phytoplankton distributions in Oregon coastal waters. *J Geophys Res* 107(C10):3174.
26. Boyle EA, Edmond JM, Sholkovitz ER (1977) The mechanism of iron removal in estuaries. *Geochim Cosmochim Acta* 41(9):1313–1324.
27. Chase Z, Strutton PG, Hales B (2007) Iron links river runoff and shelf width to phytoplankton biomass along the US West Coast. *Geophys Res Lett* 34(4):L04607.
28. Laws EA, Falkowski PB, Smith WO, Jr, Ducklow H, McCarthy JJ (2000) Temperature effects on export production in the open ocean. *Global Biogeochem Cycles* 14(4): 1231–1246.
29. Mueller PJ, Suess E (1979) Productivity, sedimentation rate, and sedimentary organic matter in the oceans, I. Organic carbon preservation. *Deep-Sea Res* 26A(12): 1347–1362.
30. Chang AS, Pedersen TF, Hendy IL (2014) Effects of productivity, glaciation, and ventilation on late Quaternary sedimentary redox and trace element accumulation on the Vancouver Island margin, western Canada. *Paleoceanography* 29(7):730–746.
31. Hartnett HE, Keil RG, Hedges JI, Devol AH (1998) Influence of oxygen exposure time on organic carbon preservation in continental margin sediments. *Nature* 391(6667): 572–574.
32. Dunne JP, Sarmiento JL, Gnanadesikan A (2007) A synthesis of global particle export from the surface ocean and cycling through the ocean interior and on the seafloor. *Global Biogeochem Cycles* 21(4):4006.
33. Kienast SS, Calvert SE, Pedersen TF (2002) Nitrogen isotope and productivity variations along the noetheast Pacific margin over the last 120 kyr: Surface and subsurface paleoceanography. *Paleoceanography* 17(4):1055.
34. Crusius J, Pedersen T, Kienast S, Keigwin L, Labeyrie L (2004) Influence of northwest Pacific productivity on North Pacific Intermediate Water oxygen concentrations during the Bøllling-Ållerød interval (14.7-12.9 ka). *Geology* 32:633–636.
35. Scholz F, McManus J, Mix AC, Hensen C, Schneider RR (2014) The impact of ocean deoxygenation on iron release from continental margin sediments. *Nat Geosci* 7:433–437.
36. Davies MH, et al. (2011) The deglacial transition on the SE Alaskan Margin: Meltwater input, sea level rise, marine productivity, and sedimentary anoxia. *Paleoceanography* 26(2):PA2223.
37. Bopp L, et al. (2013) Multiple stressors of ocean ecosystems in the 21st century: Projections with CMIP5 models. *Biogeosciences* 10(10):6225–6245.